Interaction of acoustic pressure and heat release rate fluctuations in a model rocket engine combustor

Riko Ueta, Hiroshi Gotoda ⬤,[*] Hirotaka Okamoto, and Kazuki Kawano
Department of Mechanical Engineering, Tokyo University of Science, 6-3-1 Niijuku, Katsushika-ku, Tokyo 125-8585, Japan

Takeshi Shoji ⬤ and Seiji Yoshida[†]
Japan Aerospace Exploration Agency, 7-44-1 Jindaiji-Higashimachi, Chofu-shi, Tokyo 182-8522, Japan

We experimentally clarify the interaction of acoustic pressure and heat release rate fluctuations during a transition to high-frequency combustion instability in a model rocket engine combustor. The dynamical state of acoustic pressure fluctuations undergoes a transition from high-dimensional chaotic oscillations to strongly correlated limit cycle oscillations. The coherent structure in the heat release rate field emerges with the initiation of weakly correlated limit cycle oscillations. The effect of the heat release rate on acoustic pressure fluctuations predominates during high-dimensional chaotic oscillations. In contrast, the effect of acoustic pressure on the heat release rate fluctuations markedly increases during the correlated limit cycle oscillations. These are reasonably shown by an ordinal pattern-based analysis involving the concepts of information theory, synchronization, and complex networks.

I. INTRODUCTION

Combustion instability, which is a self-sustained phenomenon resulting from the amplification of thermoacoustic resonance modes, arises in various combustors involving land-based power plants, aeroengines, and liquid rocket propulsion. In accordance with the range of the predominant frequencies of acoustic pressure fluctuations, combustion instability can be divided into three classes: low-frequency (<50 Hz), intermediate-frequency (50–1000 Hz), and high-frequency (>1000 Hz) combustion instabilities [1]. The onset and subsequent sustainment of combustion instability have detrimental effects on engine performance and finally lead to the catastrophic structural damage of combustors, through strong mechanical vibrations of the combustor and the localized increase in heat load on the combustor wall. Many theoretical and numerical studies [2–7] on the driving and sustainment mechanisms underlying high-frequency combustion instability in model rocket engine combustors have mainly examined three points: (i) the mutual coupling between the fluctuations of acoustic pressure and heat release rate; (ii) the behavior of the fuel flow velocity fluctuations induced by the propagation of acoustic pressure fluctuations in a fuel injector; and (iii) the effects of acoustic pressure and flow velocity fluctuations on flame dynamics.

The sophisticated theories of dynamical systems, synchronization, and complex networks, have recently led to a new avenue as a versatile tool to enhance our understanding of the nonlinear dynamics during high-frequency combustion instability in various model rocket engine combustors [8–12]. Aoki *et al.* [9] have carried out an experimental study on the dynamic behavior of acoustic pressure fluctuations in a cylindrical combustor with an off-center-installed coaxial injector in a model rocket engine with a single element. They observed an interesting sudden switching of two combustion states: high-dimensional chaotic oscillations with low-amplitudes and limit cycle oscillations with high-amplitudes during high-frequency intermittent combustion instability. One of the authors [10,13] has recently examined the feedback process during a transition and subsequent high-frequency combustion instability obtained by large-eddy simulation [6]. These studies [10,13] clarified that heat release rate fluctuations drive acoustic pressure fluctuations prior to the transition, whereas acoustic pressure fluctuations begin to affect heat release rate fluctuations during the transition. The directional coupling was clearly demonstrated by the transfer entropy [14] and/or symbolic transfer entropy [15]. Thus far, our experimental works [8,9] have intensively examined only the dynamic behavior of acoustic pressure fluctuations during intermittent high-frequency combustion instability. However, except for the recent studies [7,11] on intermittent high-frequency combustion instability in a model rocket engine combustor with multiple elements, the nonlinear dynamics and interaction between the acoustic and heat release rate fluctuations in a model rocket engine combustor have experimentally remained to be fully clarified.

Our main purpose in this study is to obtain a more comprehensive understanding of the nonlinear dynamics of acoustic pressure and heat release rate fluctuations during a transition to high-frequency combustion instability in a single-element rocket engine combustor by ordinal pattern-based analysis involving the concepts of information theory,

---

[*]Contact author: gotoda@rs.tus.ac.jp
[†]Contact author: yoshida.seiji@jaxa.jp

synchronization, and complex networks. We first examine the synchronized state between the acoustic pressure and heat release rate fluctuations by symbolic recurrence quantification analysis [16]. This method enables the evaluation of the similarity between two time series and has been adopted for intermediate-frequency combustion instability in a swirl-stabilized turbulent combustor [17,18]. Various classes of complex networks, such as the natural and horizontal visibility graphs [19,20], the cycle network [21], the recurrence network [16], the turbulence network [22], the ordinal partition transition network [23,24], and a spatial correlation network [25], have been widely adopted for the analysis of intermediate-frequency combustion instability [26–39]. Kasthuri *et al.* [11] have experimentally found the coherent structure of heat release rate fluctuations during intermittent high-frequency combustion instability in a model rocket engine combustor using a spatial correlation network. In this study, we examine how the coherent structure of heat release rate fluctuations emerges in the amplification process of acoustic pressure fluctuations using a symbolic recurrence plot-based network. This has not been investigated in Ref. [11]. We finally clarify the directional coupling of the acoustic pressure and heat release rate fluctuations using the symbolic transfer entropy as well as a recent numerical work [10]. The symbolic dynamics-based synchronization index [17] is an important measure for inferring the driving region of combustion instabilities [17,18,40]. We also discuss the relevance of the feedback coupling to the driving of high-frequency combustion instability by estimating the symbolic dynamics-based synchronization index [17].

This paper begins with a description of the experimental system (Sec. II), and we explain the central ideas of analytical methods in Sec. III. We present results and discussion in Sec. IV and our conclusions in Sec. V.

II. EXPERIMENTS

Figure 1(a) shows a cylindrical combustor with an off-center-installed H_2/O_2 coaxial injector [9]. The coaxial injector is located 72 mm from the center of the combustor to excite the tangential acoustic mode of high-frequency combustion instability. The diameter and length of the combustor are 200 and 500 mm, respectively. The mass flow rates of H_2 and O_2 are set to 300 and 80 L/min, respectively. The mass flow rate of N_2 issued from the face plate is set to 500 L/min to prevent the formation of H_2/air flame. Note that intermittent high-frequency combustion instability is formed under this experimental condition [9]. In this study, we focus on the amplification region of intermittent high-frequency combustion instability: a transition from stable combustion to high-frequency combustion instability (see p' in Fig. 2). We simultaneously measure the acoustic pressure fluctuations and OH^* chemiluminescence intensity fluctuations representing heat release rate fluctuations. The pressure fluctuations p' are measured by five pressure transducers (Kulite Semiconductor Products, Model ETM-375-100SG) circumferentially mounted on the wall of the combustor. The sampling frequency of p' is 102.4 kHz. There are circumferential phase differences in p' during high-frequency combustion instability among five pressure transducers. In this study, we adopt analytical methods for p' at PT1, which is close to the region of
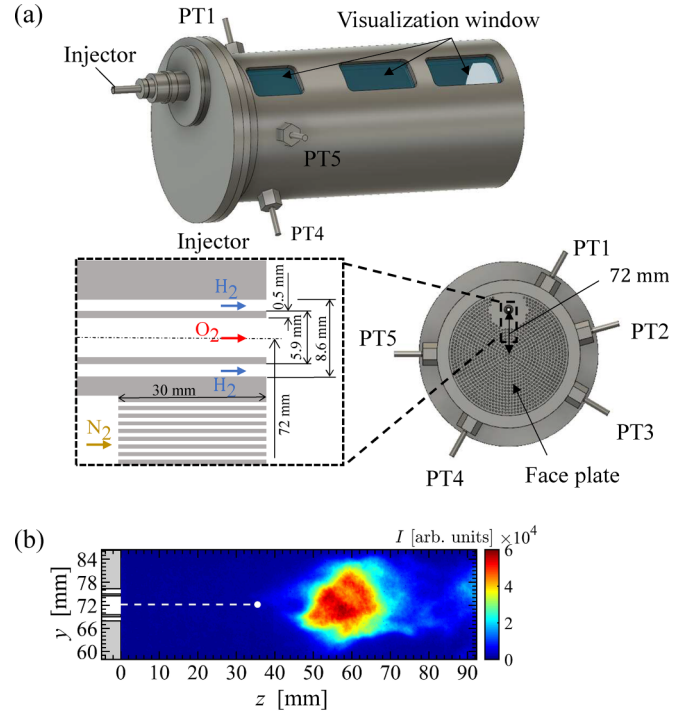

FIG. 1. (a) Experimental apparatus and (b) spatial distribution of OH^* chemiluminescence intensity.

flame formation, to appropriately capture the dynamic behavior of p'. Note that the phase difference between p' at PT1 and spatially averaged heat release rate fluctuations $\langle q' \rangle$ is nearly zero. The OH^* chemiluminescence intensity field is obtained using a high-speed video camera with an image intensifier. A bandpass filter with a center wavelength of 309.3 nm and a bandwidth of 22 nm is mounted on the front of the camera lens. The sampling frequency of q' is 20 kHz. We analyze p' at the same sampling frequency as that of q'. We also measure the flame edge location fluctuations. Here, the flame edge location is defined as the distance from the center of the O_2 injector exit ($x = z = 0$ mm and $y = 72$ mm) to the location where the OH^* chemiluminescence intensity is 20% of the maximum intensity for the time-averaged spatial distribution of q'. The flame edge location is defined in a manner similar to a numerical study [6]. Note that, in this study, the flame edge does not attach to the injector rim during high-frequency combustion instability owing to the presence of N_2 flow from the face plate.

III. ANALYTICAL METHODS

We briefly describe the central idea of the ordinal pattern-based analysis including symbolic recurrence plots, the symbolic dynamics-based synchronization index, the symbolic recurrence plot-based network, and symbolic transfer entropy.

The recurrences of the orbits in phase space based on Taken's embedding theorem [41] can be visualized as recurrence plots [42]. Symbolic sequences encoded from a time series, which are referred to as ordinal (permutation) patterns [43], were first proposed by Bandt and Pompe [44]. Symbolic
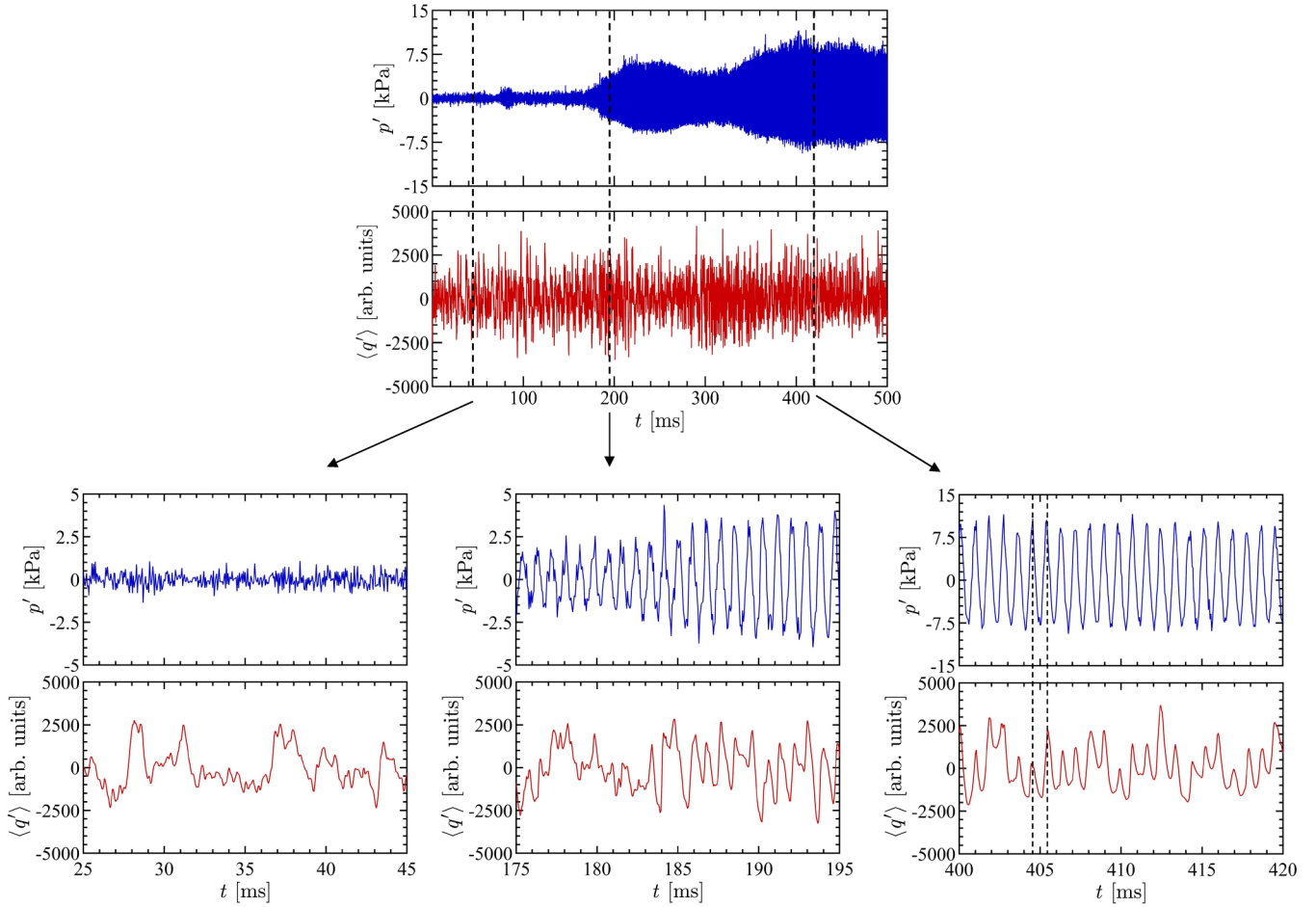
FIG. 2. Time variations in the acoustic pressure fluctuations p' and spatially averaged heat release rate fluctuations $\langle q' \rangle$ during a transition from stable combustion to high-frequency combustion instability.

recurrence plots (SRPs) [16] incorporating the Bandt-Pompe methodology into the recurrence plots enable us to evaluate the similarity of the dynamical state between two time series. The SRPs consist of the matrix element $S_{R,ij}$ as

$$S_{R,ij} = \begin{cases} 1 & \text{if } \pi_{p'}^{d_e}(t_i) = \pi_{\langle q' \rangle}^{d_e}(t_j), \\ 0 & \text{otherwise.} \end{cases} \quad (1)$$

Here, d_e is the embedding dimension of the phase space, and $\pi_{p'}^{d_e}$ and $\pi_{\langle q' \rangle}^{d_e}$ are the ordinal patterns of acoustic pressure fluctuations p' and spatially averaged heat release rate fluctuations $\langle q' \rangle$, respectively. The ordinal pattern represents the $d_e!$ possible permutations of d_e successive data points in sampled p' and $\langle q' \rangle$ at intervals of the embedding delay time τ_e. The missing ordinal patterns [45] do not appear in the permutation spectrum for a time series in white Gaussian noise with 500 data points at $d_e \leqslant 4$, which provides an important indicator for the setting of d_e suitable for constructing SRPs. Therefore, we set d_e to 4 in this study.

We estimate the symbolic recurrence rate R_{SR} representing the plot density on the diagonal line that is τ_l away from the main diagonal line ($i = j$),

$$R_{SR} = \frac{1}{N_d - |\tau_l|} \sum_{i=1}^{N_d - |\tau_l|} S_{R,ij}, \quad (2)$$

where $j = i + \tau_l$ and $N_d [= N - d_e + 1, N$ is the total number of data points in p' and $\langle q' \rangle]$ is the number of points in a d_e-dimensional phase space, which corresponds to the window length of the SRPs. R_{SR} increases as p' and $\langle q' \rangle$ become synchronized with each other. Note that an important point of utilizing SRPs is that the recurrence rate does not change regardless of the normalization or nonnormalization of p' and $\langle q' \rangle$ to [0,1]. In this study, N is set to 200, which corresponds to 10 ms of p' and $\langle q' \rangle$.

Mori *et al.* [18] have proposed the symbolic dynamics-based synchronization index as an extended version of the synchronization index [32] for inferring the driving region of intermediate-frequency combustion instability by quantifying the interaction between acoustic pressure and heat release rate fluctuations. The symbolic dynamics-based synchronization index S_{SI} considers both the phase synchronization parameter $r_{p'\langle q' \rangle}$ and the determinism D_r on SRPs. Note that the mathematical formula of $r_{p'\langle q' \rangle}$ was proposed by Gómez-Gardeñes *et al.* [46]

$$S_{SI} = D_r r_{p'\langle q' \rangle}, \quad (3)$$

$$D_r = \frac{\sum_{l=2}^{N_d - |\tau_l|} l P(l)}{\sum_{l=1}^{N_d - |\tau_l|} l P(l)}, \quad (4)$$

$$r_{p'\langle q'\rangle} = \frac{1}{N}\left|\sum_{k=1}^{N} e^{i[\theta_{p'}(t_k)-\theta_{\langle q'\rangle}(t_k)]}\right|, \quad (5)$$

where l is the length of the diagonal line that is τ_l away from the main diagonal line, $P(l)$ is the frequency distribution of l, and $\theta_{p'}(t_k)$ and $\theta_{\langle q'\rangle}(t_k)$ are, respectively, the instantaneous phases of p' and $\langle q'\rangle$ at time t_k. $r_{p'\langle q'\rangle}$ quantifies the degree of phase synchronization. Note that $D_r \approx 1$ means the formation of the in-phase synchronized state. S_{SI} becomes high as p' and $\langle q'\rangle$ are coupled to each other. In this study, we set $d_e = 4$, $N_d = 498$, and $N = 500$.

Kasthuri *et al.* [11] showed that the spatial network based on the two-point correlation between the spatial grid points of the observation domain can clarify the coherent structure of heat release rate fluctuations during combustion instability. In this study, we propose a new symbolic recurrence plot-based network to evaluate the coherency in heat release rate field. We construct the network using D_r of the principal diagonal $S_{R,mn}$ on SRPs

$$S_{R,mn} = \begin{cases} 1 & \text{if } \pi_{\langle q_m\rangle}^{d_e}(t_k) = \pi_{\langle q_n\rangle}^{d_e}(t_k), \\ 0 & \text{otherwise.} \end{cases} \quad (6)$$

Here, $\pi_{\langle q_m\rangle}^{d_e}(t_k)$ is the ordinal pattern of $q(t_k)$ at a node m in the network. A node corresponds to the second-order moment [31] of OH* chemiluminescence intensity in terms of y at a z location. We define the adjacency matrix with element A_{ij} of the network. $A_{ij} = 1$ for $D_r \geqslant \alpha$, whereas $A_{ij} = 0$ for $D_r < \alpha$, where $0 \leqslant D_r \leqslant 1$. We estimate the degree centrality $C_{k,i}$ and the closeness centrality $C_{l,i}$ in the network

$$C_{k,i} = \frac{k_i}{N_v - 1}, \quad (7)$$

$$C_{l,i} = \frac{N_v - 1}{\sum_{j=1, j\neq i}^{N_v} d_{ij}}, \quad (8)$$

where k_i is the degree of node i, N_v is the total number of nodes, d_{ij} is the distance between the pair nodes i and j, $0 \leqslant C_{k,i} \leqslant 1$, and $0 \leqslant C_{l,i} \leqslant 1$. A high $C_{k,i}$ means that a node i is adjacent to many nodes, whereas a high $C_{l,i}$ means that a node i is connected to all the other nodes with short paths in the network. In this study, d_e, N_v, and α are set to 4, 467, and 0.7, respectively.

Various causality measures, such as the Granger causality [47,48], transfer entropy [14], symbolic transfer entropy [15], and cross convergent mapping [49], have been proposed to clarify the directed interaction between possibly coupled dynamic behaviors. The transfer entropy based on information theory is a prevailing measure, but it requires the setting of many parameters used as thresholds for constructing the distribution in the joint and conditional probabilities of the variables. In contrast, the symbolic transfer entropy incorporating ordinal patterns in a time series does not require the setting of many parameters. Shima *et al.* [10] adopted the symbolic transfer entropy for the acoustic pressure and heat release rate fluctuations obtained by large-eddy simulation. They showed that the symbolic transfer entropy is valid for clarifying their directional coupling in a model rocket engine combustor. In this study, we estimate the

directionality index ΔS_S defined as the difference between the symbolic transfer entropies as

$$\Delta S_{S,p'\to\langle q'\rangle} = S_{S,p'\to\langle q'\rangle} - S_{S,\langle q'\rangle\to p'}, \quad (9)$$

$$S_{S,p'\to\langle q'\rangle} = \sum_m P\big(\pi_{\langle q'\rangle}^{d_e}(t_{m+1}), \pi_{\langle q'\rangle}^{d_e}(t_m), \pi_{p'}^{d_e}(t_m)\big)$$

$$\times \log_2 \frac{P\big(\pi_{\langle q'\rangle}^{d_e}(t_{m+1})|\pi_{\langle q'\rangle}^{d_e}(t_m), \pi_{p'}^{d_e}(t_m)\big)}{P\big(\pi_{\langle q'\rangle}^{d_e}(t_{m+1})|\pi_{\langle q'\rangle}^{d_e}(t_m)\big)}, \quad (10)$$

where $S_{S,p'\to\langle q'\rangle}$ is the symbolic transfer entropy for the direction of p' to $\langle q'\rangle$. $\pi_{p'}^{d_e}(t_m)$ is the ordinal pattern of p' and $\pi_{\langle q'\rangle}^{d_e}(t_m)$ is the ordinal pattern of $\langle q'\rangle$ at a time t_m. $P(\pi_{\langle q'\rangle}^{d_e}(t_{m+1}), \pi_{\langle q'\rangle}^{d_e}(t_m), \pi_{p'}^{d_e}(t_m))$ is the joint probability of $\pi_{\langle q'\rangle}^{d_e}(t_{m+1})$, $\pi_{\langle q'\rangle}^{d_e}(t_m)$, and $\pi_{p'}^{d_e}(t_m)$. $P(\pi_{\langle q'\rangle}^{d_e}(t_{m+1})|\pi_{\langle q'\rangle}^{d_e}(t_m))$ is the conditional probability of $\pi_{\langle q'\rangle}^{d_e}(t_{m+1})$ given $\pi_{\langle q'\rangle}^{d_e}(t_m)$. $\Delta S_{S,p'\to\langle q'\rangle}$ takes a negative value when the information flow from $\langle q'\rangle$ to p' is relatively stronger than the opposite information flow. In this study, d_e and N are respectively set to 3 and 500 corresponding to approximately 25 cycles of high-frequency combustion instability to satisfy $(d_e!)^3 < N$, where N is the total number of data points in p' and $\langle q'\rangle$. Note that the relation equation between d_e and N corresponds to the condition for calculating the joint probability of $\pi_{\langle q'\rangle}^{d_e}(t_{m+1})$, $\pi_{\langle q'\rangle}^{d_e}(t_m)$, and $\pi_{p'}^{d_e}(t_m)$.

IV. RESULTS AND DISCUSSION

Figure 2 shows the time variations in acoustic pressure fluctuations p' and spatially averaged heat release rate fluctuations $\langle q'\rangle$ during a transition from stable combustion to high-frequency combustion instability. p' notably amplifies with an amplitude of approximately ± 6 kPa during stable combustion at 160 ms $\leqslant t \leqslant 210$ ms. We observe a further increase in the amplitude of p' up to approximately ± 10 kPa at 320 ms $\leqslant t \leqslant 400$ ms, leading to high-frequency combustion instability. We also observe the emergence of strong periodic oscillations in $\langle q'\rangle$ during high-frequency combustion instability. p' and $\langle q'\rangle$ behave in phase. An interesting point to note here is that in contrast to sinusoidal p', $\langle q'\rangle$ exhibits a large amplitude modulation. Time variations in the power spectrum of p' and $\langle q'\rangle$ during a transition from stable combustion to high-frequency combustion instability are shown in Fig. 3. A dominant peak of p' with approximately 1100 Hz appears in the power spectrum during stable combustion state, which corresponds to the first tangential (1T) acoustic mode of the combustor. Note that we ensured the excitation of the 1T mode for other pressure transducers. We observe the same dominant peak of $\langle q'\rangle$ with p' during stable combustion state. The harmonics of the 1T acoustic mode with approximately 2200 Hz clearly appears in the power spectrum during high-frequency combustion instability. Aoki *et al.* [9] have examined the existence of chaos in acoustic pressure fluctuations during stable combustion at a different oxygen flow rate using two analytical methods: a multiscale complexity-entropy causality plane method in terms of symbolic dynamics [50] and a local nonlinear prediction method [51,52]. Gao *et al.* [53–55] have proposed the scale-dependent Lyapunov exponent (SDLE) to discriminate chaos and stochastic dynamics. The applicability
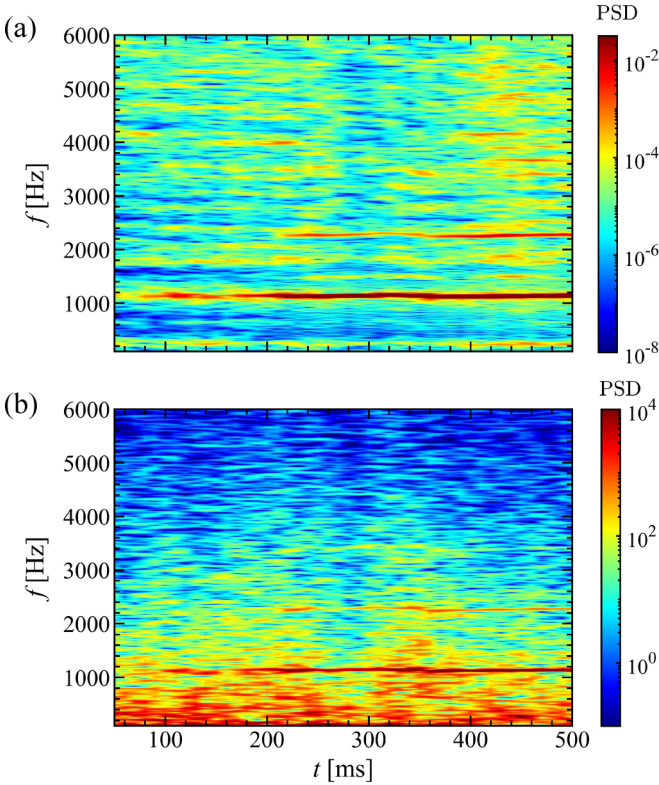
(a)

(b)

FIG. 3. Time variations in power spectrum density of (a) p' and (b) $\langle q' \rangle$ during a transition from stable combustion to high-frequency combustion instability.

of the SDLE has been shown in a different combustion system [56]. Similar to Refs. [53–55], we thus attempt to obtain additional evidence for the existence of chaos in p' during stable combustion by estimating the SDLE. In this method, we first set the initial separation ϵ_0 of two nearby orbits in d_e-dimensional phase space, where $\epsilon_k \leqslant \epsilon_0 \leqslant \epsilon_k + \Delta\epsilon_k$ and ϵ_k is the shell size in the phase space. SDLE is estimated as $\lambda(\epsilon_t)(=\langle \ln \epsilon_{t+\Delta t} - \ln \epsilon_t \rangle / \Delta t$, where ϵ_t and $\epsilon_{t+\Delta t}$ are respectively the average separations between two nearby orbits at times t and $t + \Delta t$, and Δt is the sampling time of p'). In this study, d_e and τ_e are set to 4 and 0.2 ms, respectively. Here, the suitable value of τ_e is determined by the mutual information [57]. Note that the shell size is set to $(2^{-2}, 2^{-5/2})$. The variation in λ against ϵ is shown in Fig. 4. λ exhibits a plateau-like behavior and is approximately 3.0 [1/ms], indicating the existence of chaos. This supports the finding obtained by Aoki *et al.* [9].

Figure 5 shows the time variations in the amplitude of flame edge location fluctuations A_m and the power spectrum density of flame edge location fluctuations. A_m remains nearly unchanged at $t \leqslant 175$ ms and gradually increases with time at $t \geqslant 200$ ms corresponding to the variation in p'. We observe the appearance of a dominant peak in the power spectrum density. The frequency of the dominant peak is nearly the same as that of p' (see Fig. 3). On the basis of a numerical study [6], these results indicate that the large change in the amplitude of flame edge location fluctuations is significantly associated with the excitation of the 1T mode leading to high-frequency combustion instability.
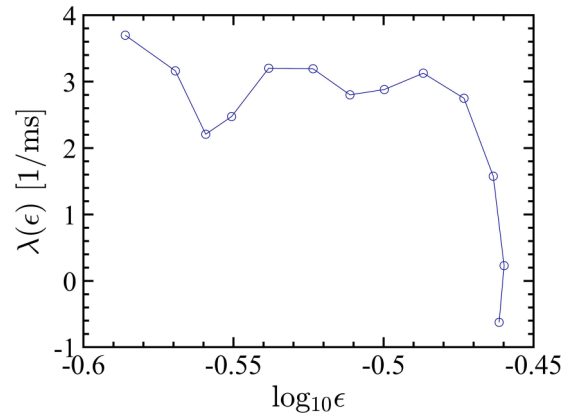

FIG. 4. Variation in Lyapunov exponent λ against shell size ϵ for p' during stable combustion.

Figure 6 shows the time variation in the recurrence rate R_{SR}, together with the expanded SRPs at representative combustion states: stable combustion, transitional region corresponding to the amplification region of acoustic pressure fluctuations, and well-developed high-frequency combustion instability. Here, τ_a corresponds to the actual delay time ($=\tau_l\Delta t$, where Δt is the time resolution of p' and $\langle q' \rangle$). The ordinal pattern expressing an increasing (decreasing) process of both p' and $\langle q' \rangle$ is displayed as a red (blue) plot. Note that the length of the recurrence points displayed in the rectangular configuration corresponds to the formation time of the ordinal patterns. As shown in Fig. 6(a), we observe the recurrence points consisting of various ordinal patterns. Their sizes are not constant during stable combustion. R_{SR} takes low values. These results indicate the nearly desynchronized state between p' and $\langle q' \rangle$. Regularly arrayed structures with
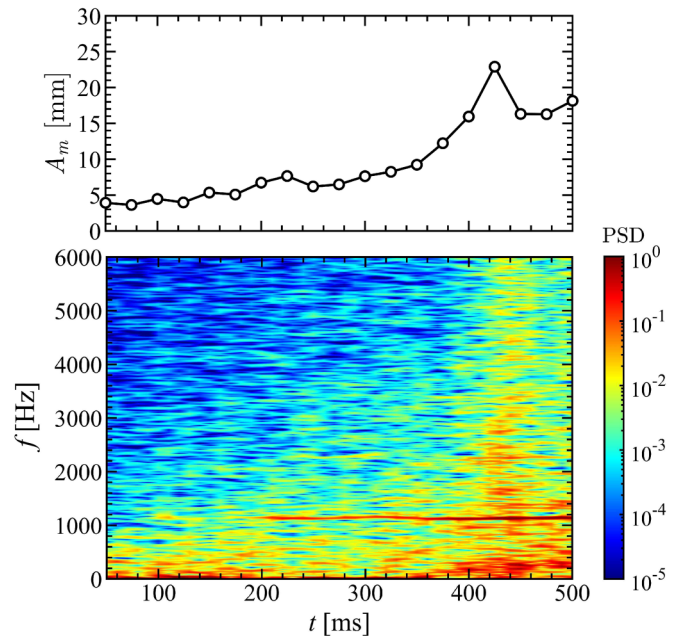

FIG. 5. Time variations in the amplitude of flame edge location fluctuations A_m and the power spectrum density of flame edge location fluctuations.
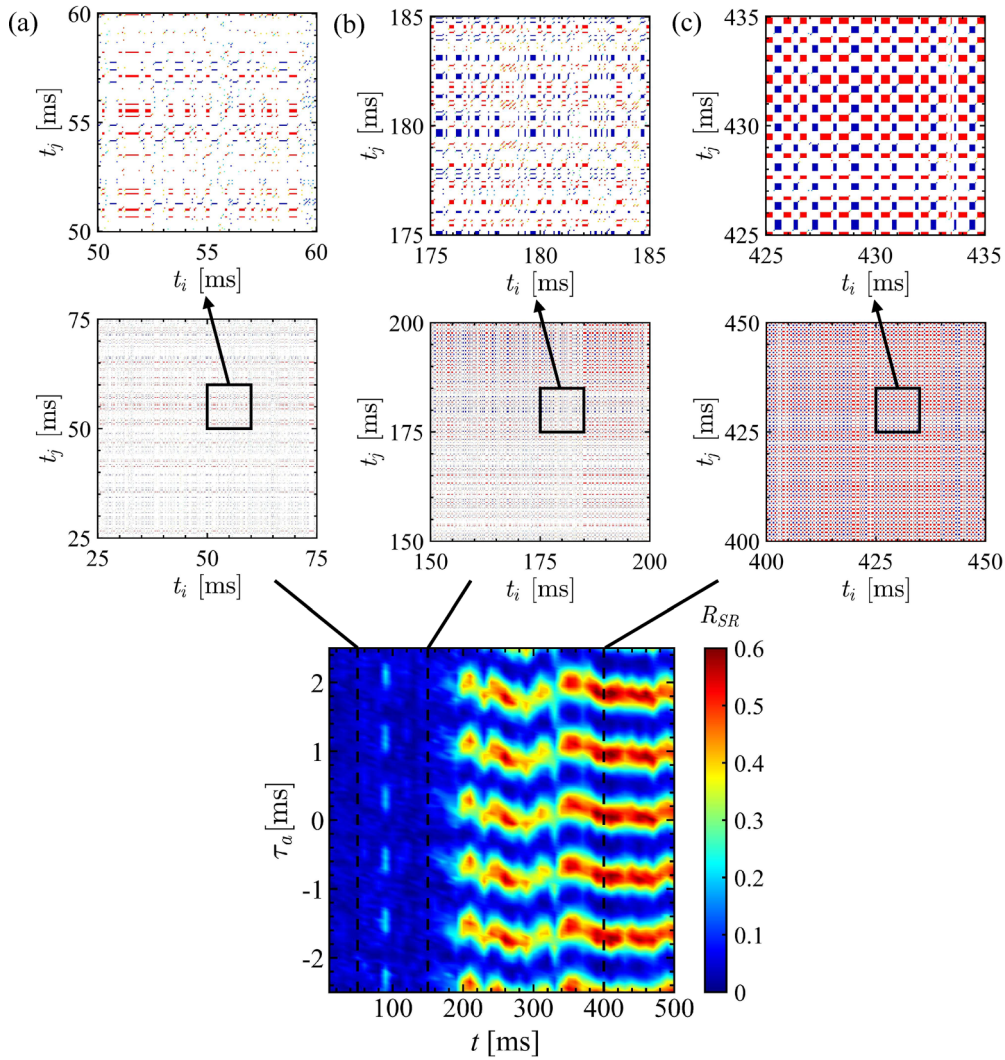
FIG. 6. Time variation in the recurrence rate R_{SR}, together with the expanded SRPs at representative combustion states: stable combustion, transitional region corresponding to the amplification region of acoustic pressure fluctuations, and well-developed combustion instability.

a larger length of the recurrence points begin to appear in the transitional region, showing a significant increase in R_{SR}. The number of points in SRPs is also larger than those during stable combustion. These indicate the emergence of the synchronized state between p' and $\langle q' \rangle$. We observe that R_{SR} takes maximum values with an interval of $\tau_a \approx 1$ ms. This time interval coincides with the period of the 1T acoustic mode. Two patterns corresponding to the increasing and decreasing processes are predominant during well-developed high-frequency combustion instability. We observe the notable increase in the length of the recurrence points, maintaining high R_{SR}. R_{SR} takes a high value at $\tau_a \sim 0$ ms, showing the formation of the in-phase synchronized state between p' and $\langle q' \rangle$ during high-frequency combustion instability. Gao [58] has studied the recurrence time in the recurrence plots (RPs) constructed from single chaotic time series data produced by a nonlinear dynamical system. He examined the relevance of the recurrence time in the RPs and the maximal Lyapunov exponent. Gao and Cai [59] have also shown that a rectangle-like structure appears when sojourn points are present in the attractor. In this study, we have examined the changes in synchronized

state using the SRPs constructed from multiple time series data. In relation to the identification of chaos in acoustic pressure fluctuations using the SDLE, it would be interesting to elucidate how the recurrence time statics in the SRPs constructed from a single time series are useful for detecting the dynamical changes during a transition to high-frequency combustion instability.

Figure 7 shows the variations in the recurrence rate of acoustic pressure fluctuations $R_{SR,p'}$ and that of heat release rate fluctuations $R_{SR,\langle q' \rangle}$ in terms of τ_a for representative combustion states of stable combustion, the transitional region, and well-developed high-frequency combustion instability. Note that $R_{SR,p'}$ ($R_{SR,\langle q' \rangle}$) increases as the autocorrelation appears in p' ($\langle q' \rangle$). $R_{SR,p'}$ and $R_{SR,\langle q' \rangle}$ during stable combustion fluctuate irregularly as a function of τ_a. The mean $R_{SR,p'}$ ($R_{SR,\langle q' \rangle}$) is approximately 0.05 (0.18), indicating a weak autocorrelation of p' ($\langle q' \rangle$). The variation in $R_{SR,p'}$ does not match that in $R_{SR,\langle q' \rangle}$. These results suggest that p' and $\langle q' \rangle$ are desynchronized each other without possessing the autocorrelation. $R_{SR,p'}$ and $R_{SR,\langle q' \rangle}$ start to fluctuate periodically during the transitional region. We observe the
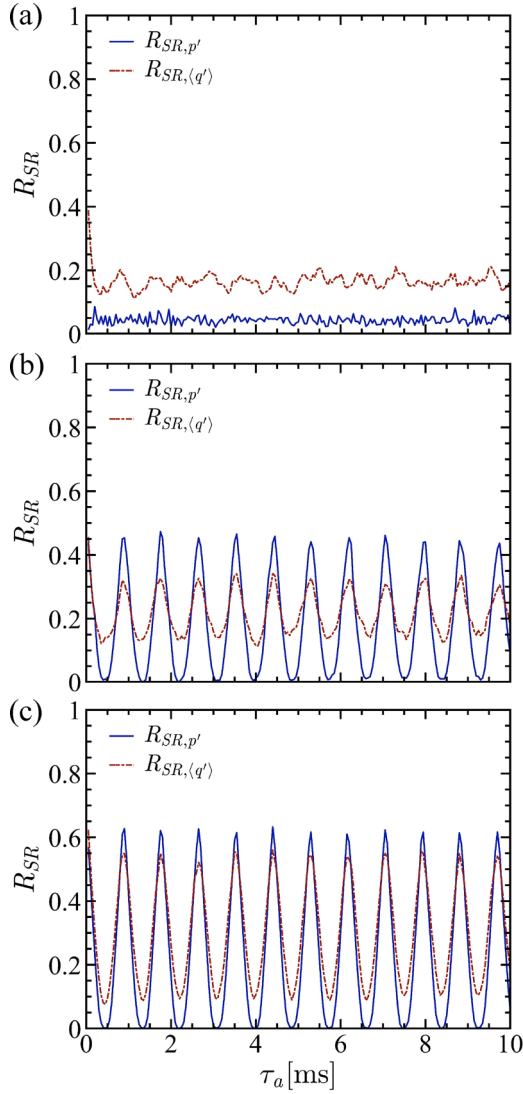
FIG. 7. Variations in the recurrence rate of the acoustic pressure fluctuations $R_{SR,p'}$ and heat release rate fluctuations $R_{SR,\langle q'\rangle}$ in terms of actual delay time τ_a. Here, (a) stable combustion at 25 ms $\leqslant t \leqslant$ 75 ms, (b) transitional region at 175 ms $\leqslant t \leqslant$ 225 ms, and (c) well-developed combustion instability at 400 ms $\leqslant t \leqslant$ 450 ms.

increases in the local maximal values of $R_{SR,p'}$ and $R_{SR,\langle q'\rangle}$ in terms of τ_a and the locking of the local maximum location in $R_{SR,p'}$ and $R_{SR,\langle q'\rangle}$, indicating the appearance of autocorrelation in p' and $\langle q'\rangle$. However, their local maximum values do not match with each other. Pawar *et al.* [60] and Godavarthi *et al.* [30] have recently distinguished the dynamical state of intermediate-frequency combustion instability in a bluff-body-type turbulent combustor: a weakly correlated limit cycle and a strongly correlated limit cycle by evaluating the probability of recurrence on the recurrence plots in terms of delay time. The former dynamical state is induced by phase synchronization and the latter by generalized synchronization. They showed that the dynamical state represents weakly correlated limit cycle oscillations when the local maximal value of the periodically oscillating probability of recurrence in the acoustic pressure fluctuations does not fit well with that in the heat release rate fluctuations. On this basis, the
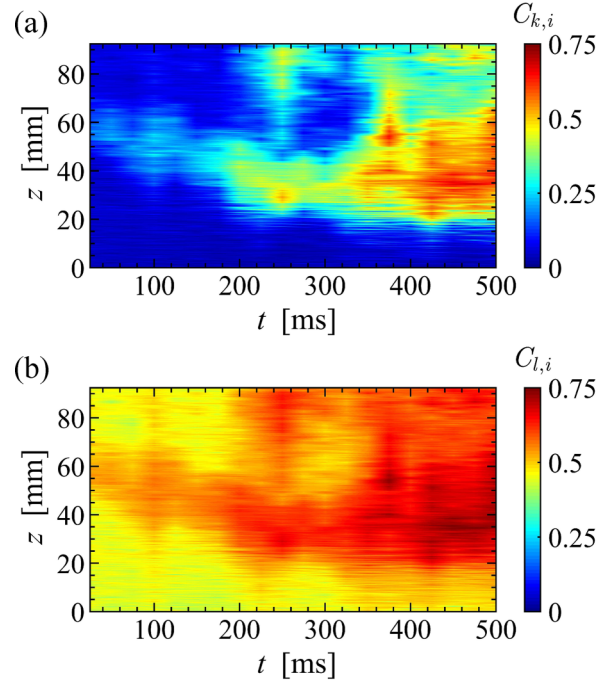

FIG. 8. Time variations in the degree centrality $C_{k,i}$ and closeness centrality $C_{l,i}$ in symbolic recurrence plot-based network.

dynamical state of the transitional region represents the weakly correlated limit cycle oscillations. We observe the strong periodicity of both $R_{SR,p'}$ and $R_{SR,\langle q'\rangle}$ with high magnitudes of local maximal values during well-developed high-frequency combustion instability. The local maximal values of $R_{SR,p'}$ nearly coincide with those of $R_{SR,\langle q'\rangle}$, indicating that the dynamical state of well-developed high-frequency combustion instability represents the strongly correlated limit cycle oscillations.

Figure 8 shows the time variations in the degree centrality $C_{k,i}$ and closeness centrality $C_{l,i}$. $C_{k,i}$ notably begins to increase at $t \approx 200$ ms corresponding to the formation region of weakly correlated limit cycle oscillations. We clearly observe the expansion of the high $C_{k,i}$ region when A_m significantly increases owing to the emergence of strongly correlated limit cycles. The high values of $C_{k,i}$ mean the strong determinism in the connections between the nodes in the network, indicating the formation of a coherent structure. $C_{l,i}$ shows a similar trend to $C_{k,i}$. An important point to note here is that there are no clear differences between the two centralities. This shows that the network representing heat release regions simultaneously contains the two characteristics. The high values of $C_{l,i}$ correspond to the core region of the coherent structure. These centralities are useful for deducing the formation and core regions of the coherent structure. The results obtained in Fig. 8 suggest that the coherent structure in heat release rate field emerges with the initiation of weakly correlated limit cycle oscillations. The formation region of the coherent structure widely broadens as t exceeds approximately 400 ms corresponding to the onset of strongly correlated limit cycle oscillations. These results demonstrate that the transition to high-frequency combustion instability is strongly associated with the emergence of the coherent structure in heat release

rate field. We here mention an important advantage of the symbolic recurrence plot-based network. As shown in Fig. 2, p' nearly behaves sinusoidally, whereas $\langle q' \rangle$ exhibits a large amplitude modulation during high-frequency combustion instability. The correlation coefficient used to construct a spatial network can poorly evaluate the similarity between $\langle q_m \rangle$ and $\langle q_n \rangle$ dominated by phase synchronization. In contrast, the symbolic dynamics-based ordinal patterns [44] in a time series can evaluate the degree of coincidence of a phase between $\langle q_m \rangle$ and $\langle q_n \rangle$ even with a large amplitude modulation in $\langle q' \rangle$. This is an important point for the appropriate capture of the coherent structure in the heat release rate field.

In relation to pattern formation in turbulent thermoacoustic systems, we discuss the emergence of the coherent structure in heat release rate field in the transitional region. Spatially ordered structures resulting from collective interaction emerge in a self-driven system [61]. On the basis of this concept, Sujith *et al.* [62,63] have recently revealed the relevance of large-scale vortical motion to the coherence in acoustic power field during intermediate combustion instability in a bluff-body turbulent combustor. They showed that the collective interaction of small-scale vorticies shed in the shear layer region induces an organized large-scale vortex in a confined thermoacoustic system, resulting in the spatially ordered coherency in heat release rate field leading to the onset of combustion instability. Hashimoto *et al.* [13] numerically showed that large flame edge fluctuations induce a large-scale vortex arising from small-scale vortices in the shear layer region between H_2 and O_2 jets during high-frequency combustion instability. On this basis, a similar argument in recent studies [62,63] may apply to the emergence of coherency in heat release rate field during a transition to high-frequency combustion instability, although we have yet to experimentally clarify the vortical structure in the shear layer region between H_2 and O_2 jets in our combustor.

Figure 9 shows the time variations in the symbolic dynamics-based synchronization index S_{SI} and the directionality index $\Delta S_{S,p' \to \langle q' \rangle}$. S_{SI} is approximately 0.1 during high-dimensional chaotic oscillations, indicating the nearly decoupled p' and $\langle q' \rangle$. It takes approximately 0.7 during strongly correlated limit cycle oscillations, showing the strong coupling of p' and $\langle q' \rangle$. Note that $S_{S_{SI}}$ is approximately 0.25 at $t = 100$ ms owing to the transient increase in the amplitude of p'. However, the drop in S_{SI} occurs at approximately 125 ms. We observe a decrease in the magnitude of p' compared with the amplitude of p' at approximately 80 ms. This indicates a temporary recovery from weakly correlated limit cycle oscillations to high-dimensional chaotic oscillations. $\Delta S_{S,p' \to \langle q' \rangle}$ is less than zero at $t \leqslant 100$ ms corresponding to stable combustion, which shows that the information flow from $\langle q' \rangle$ to p' is relatively stronger than the opposite information flow. The sign of $\Delta S_{S,p' \to \langle q' \rangle}$ remains negative at $t \leqslant 225$ ms, but $\Delta S_{S,p' \to \langle q' \rangle}$ markedly increases at 150 ms $\leqslant t \leqslant 225$ ms. This means that $\langle q' \rangle$ strongly affects p', whereas the effect of p' on $\langle q' \rangle$ gradually increases in the subsequent transitional region. In contrast, $\Delta S_{S,p' \to \langle q' \rangle}$ becomes positive at $t \geqslant 250$ ms, which indicates that the opposite directional coupling notably affects the feedback loop during high-frequency combustion instability. The significant change in the sign of $\Delta S_{S,p' \to \langle q' \rangle}$ reasonably corresponds to that obtained by numerical

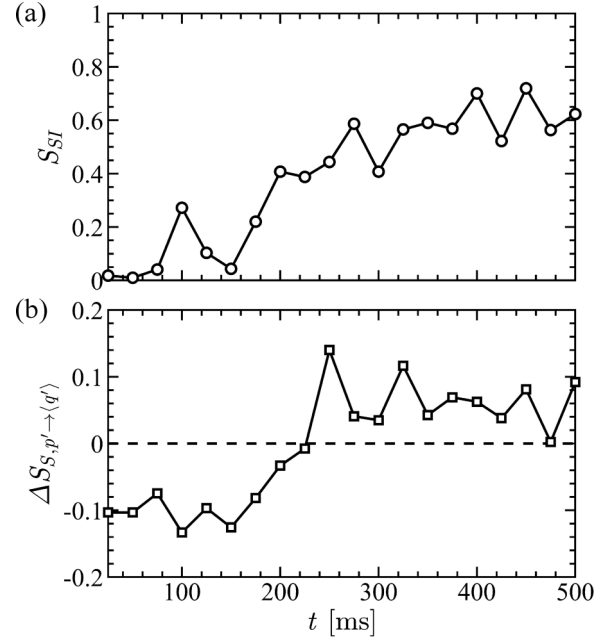FIG. 9. Time variations in the symbolic dynamics-based synchronization index S_{SI} and the directionality index $\Delta S_{S,p' \to \langle q' \rangle}$.

computation [10]. Another important point drawn from Fig. 7 is that S_{SI} is approximately 0.37 when the sign of $\Delta S_{S,p' \to \langle q' \rangle}$ markedly changes at $t = 225$ ms. This gives us a threshold of the symbolic dynamics-based synchronization index to determine the onset of high-frequency combustion instability. Other causality measures such as cross transitivity [64] in the recurrence network have been adopted to identify the directed interaction of acoustic pressure and heat release rate fluctuations in a bluff-body-type combustor [30] and acoustic pressure fluctuations between coupled multiple combustors [65]. The causality analysis including the symbolic transfer entropy will become an important approach to examining the degree of bidirectional coupling in various dynamical states emerging in thermoacoustic systems.

Thus far, the importance of symbolic dynamics for investigating the nonlinear determinism in aperiodic fluctuations has been shown in not only thermoacoustic systems [17,29,31,66–68] but also various physical settings: flame front instability induced by buoyancy/swirl coupling [69], buoyancy-driven turbulent flame [56,70,71], and propagating flame in a Hele–Shaw cell [72,73]. The ordinal pattern-based analysis we adopted in this study would be helpful for understanding the interaction of acoustic pressure and heat release rate fluctuations during a transition to high-frequency combustion instability in a model rocket combustor, including the characterization of dynamical states.

V. CONCLUSION

We have experimentally studied the nonlinear dynamics of acoustic pressure and heat release rate fluctuations during a transition to high-frequency combustion instability in a model rocket engine combustor by ordinal pattern-based analysis involving the concepts of information theory, synchronization, and complex networks. The model combustor

consists of a cylindrical combustor with an off-center-installed coaxial single-element H_2/O_2 injector. We observe a significant change in dynamical state from high-dimensional chaotic oscillations to strongly correlated limit cycle oscillations during high-frequency combustion instability via weakly correlated limit cycle oscillations in the transitional region. The desynchronized state between the acoustic pressure and heat release rate fluctuations is formed during high-dimensional chaotic oscillations. It changes to nearly generalized synchronization during high-frequency combustion instability via phase synchronization in the transitional region. These are reasonably identified by the recurrence rate on SRPs. The amplitude of the flame edge location fluctuations significantly increases as the acoustic pressure fluctuations amplify in the transitional region from high-dimensional chaotic oscillations to strongly-correlated limit cycle oscillations. The large fluctuations in the flame edge location

exciting the 1T acoustic mode of the combustor play an important role in the emergence of the coherent structure in heat release rate field. This is clarified by the symbolic recurrence plot-based network we proposed in this study. The effect of heat release rate on acoustic pressure fluctuations relatively predominates during high-dimensional chaotic oscillations. In contrast, the effect of acoustic pressure on heat release rate fluctuations markedly increases during correlated limit cycle oscillations. This is demonstrated by the symbolic transfer entropy. The change in directionality between heat release rate and acoustic pressure fluctuations is qualitatively in agreement with that obtained by numerical computation [13].

ACKNOWLEDGMENT

[1] T. C. Lieuwen and V. Yang, *Combustion Instabilities in Gas Turbine Engines: Operational Experience, Fundamental Mechanisms and Modeling* (American Institute of Aeronautics and Astronautics, Reston, VA, 2005).

[2] W. Armbruster, J. S. Hardi, and M. Oschwald, Proc. Combust. Inst. **38**, 5963 (2021).

[3] A. Urbano, Q. Douasbin, L. Selle, G. Staffelbach, B. Cuenot, T. Schmitt, S. Ducruix, and S. Candel, Proc. Combust. Inst. **36**, 2633 (2017).

[4] C. J. Morgan, K. J. Shipley, and W. E. Anderson, J. Propul. Power **31**, 1696 (2015).

[5] M. E. Harvazinski, C. Huang, V. Sankaran, T. W. Feldman, W. E. Anderson, C. L. Merkle, and D. G. Talley, Phys. Fluids **27**, 045102 (2015).

[6] S. Matsuyama, D. Hori, T. Shimizu, S. Tachibana, S. Yoshida, and Y. Mizobuchi, J. Propul. Power **32**, 628 (2016).

[7] P. Kasthuri, S. A. Pawar, R. Gejji, W. Anderson, and R. I. Sujith, Combust. Flame **240**, 112047 (2022).

[8] H. Kasuya, H. Gotoda, S. Yoshida, and S. Tachibana, Chaos **28**, 033111 (2018).

[9] C. Aoki, H. Gotoda, S. Yoshida, and S. Tachibana, J. Appl. Phys. **127**, 224903 (2020).

[10] S. Shima, K. Nakamura, H. Gotoda, Y. Ohmichi, and S. Matsuyama, Phys. Fluids **33**, 064108 (2021).

[11] P. Kasthuri, A. Krishnan, R. Gejji, W. Anderson, N. Marwan, J. Kurths, and R. I. Sujith, Phys. Fluids **34**, 034107 (2022).

[12] K. Kawano, H. Gotoda, Y. Nabae, Y. Ohmichi, and S. Matsuyama, J. Fluid Mech. **959**, A1 (2023).

[13] T. Hashimoto, H. Shibuya, H. Gotoda, Y. Ohmichi, and S. Matsuyama, Phys. Rev. E **99**, 032208 (2019).

[14] T. Schreiber, Phys. Rev. Lett. **85**, 461 (2000).

[15] M. Staniek and K. Lehnertz, Phys. Rev. Lett. **100**, 158101 (2008).

[16] N. Marwan, M. C. Romano, M. Thiel, and J. Kurths, Phys. Rep. **438**, 237 (2007).

[17] K. Asami, T. Kawada, S. Kishiya, and H. Gotoda, Europhys. Lett. **139**, 13001 (2022).

[18] Y. Mori, T. Kawada, S. Fukuda, and H. Gotoda, Proc. Combust. Inst. **39**, 4671 (2023).

[19] L. Lacasa, B. Luque, F. Ballesteros, J. Luque, and J. C. Nũno, Proc. Natl. Acad. Sci. USA **105**, 4972 (2008).

[20] L. Lacasa and R. Toral, Phys. Rev. E **82**, 036120 (2010).

[21] J. Zhang and M. Small, Phys. Rev. Lett. **96**, 238701 (2006).

[22] K. Taira, A. G. Nair, and S. L. Brunton, J. Fluid Mech. **795**, R2 (2016).

[23] M. McCullough, M. Small, T. Stemler, and H. H.-C. Iu, Chaos **25**, 053101 (2015).

[24] J. Zhang, J. Zhou, M. Tang, H. Guo, M. Small, and Y. Zou, Sci. Rep. **7**, 7795 (2017).

[25] G. Iacobello, S. Scarsoglio, J. G. M. Kuerten, and L. Ridolfi, Phys. Rev. E **98**, 013107 (2018).

[26] M. Murugesan and R. I. Sujith, J. Fluid Mech. **772**, 225 (2015).

[27] Y. Okuno, M. Small, and H. Gotoda, Chaos **25**, 043107 (2015).

[28] H. Gotoda, H. Kinugawa, R. Tsujimoto, S. Domen, and Y. Okuno, Phys. Rev. Appl. **7**, 044027 (2017).

[29] Y. Guan, M. Murugesan, and L. K. B. Li, Chaos **28**, 093109 (2018).

[30] V. Godavarthi, S. A. Pawar, V. R. Unni, R. I. Sujith, N. Marwan, and J. Kurths, Chaos **28**, 113111 (2018).

[31] S. Murayama, H. Kinugawa, I. T. Tokuda, and H. Gotoda, Phys. Rev. E **97**, 022223 (2018).

[32] S. Murayama and H. Gotoda, Phys. Rev. E **99**, 052222 (2019).

[33] T. Kobayashi, S. Murayama, T. Hachijo, and H. Gotoda, Phys. Rev. Appl. **11**, 064034 (2019).

[34] Y. Guan, L. K. B. Li, B. Ahn, and K. T. Kim, Chaos **29**, 053124 (2019).

[35] A. Krishnan, R. I. Sujith, N. Marwan, and J. Kurths, J. Fluid Mech. **874**, 455 (2019).

[36] R. I. Sujith and V. R. Unni, Phys. Fluids **32**, 061401 (2020).

[37] Y. Guan, V. Gupta, and L. K. B. Li, J. Fluid Mech. **894**, R3 (2020).

[38] A. Krishnan, R. I. Sujith, N. Marwan, and J. Kurths, J. Fluid Mech. **916**, A20 (2021).

[39] T. Kurosaka, S. Masuda, and H. Gotoda, Chaos **31**, 073121 (2021).

[40] K. Baba, S. Kishiya, H. Gotoda, T. Shoji, and S. Yoshida, Chaos **33**, 073101 (2023).

[41] F. Takens, *Dynamical Systems and Turbulence, Warwick 1980*, Lecture Notes in Mathematics Vol. 898 (Springer, Berlin, 1981), p. 366.

[42] J. Eckmann, S. O. Kamphorst, and D. Ruelle, Europhys. Lett. **4**, 973 (1987).

[43] J. M. Amigó, *Permutation Complexity in Dynamical Systems: Ordinal Patterns, Permutation Entropy and All That* (Springer Science and Business Media, New York, 2010).

[44] C. Bandt and B. Pompe, Phys. Rev. Lett. **88**, 174102 (2002).

[45] C. W. Kulp and L. Zunino, Chaos **24**, 033116 (2014).

[46] J. Gómez-Gardeñes, Y. Moreno, and A. Arenas, Phys. Rev. Lett. **98**, 034101 (2007).

[47] C. W. J. Granger, Econometrica **37**, 424 (1969).

[48] L. Barnett, A. B. Barrett, and A. K. Seth, Phys. Rev. Lett. **103**, 238701 (2009).

[49] G. Sugihara, R. May, H. Ye, C. Hsieh, E. Deyle, M. Fogarty, and S. Munch, Science **338**, 496 (2012).

[50] L. Zunino, M. C. Soriano, and O. A. Rosso, Phys. Rev. E **86**, 046210 (2012).

[51] H. Gotoda, Y. Shinoda, M. Kobayashi, Y. Okuno, and S. Tachibana, Phys. Rev. E **89**, 022910 (2014).

[52] H. Gotoda, M. Pradas, and S. Kalliadasis, Phys. Rev. Fluids **2**, 124401 (2017).

[53] J. B. Gao, J. Hu, W. W. Tung, and Y. H. Cao, Phys. Rev. E **74**, 066204 (2006).

[54] J. B. Gao, Y. H. Cao, W. W. Tung, and J. Hu, *Multiscale Analysis of Complex Time Series* (Wiley, New York, 2007).

[55] W. W. Tung, J. Gao, J. Hu, and L. Yang, Phys. Rev. E **83**, 046210 (2011).

[56] K. Takagi, H. Gotoda, I. T. Tokuda, and T. Miyano, Phys. Rev. E **96**, 052223 (2017).

[57] A. M. Fraser and H. L. Swinney, Phys. Rev. A **33**, 1134 (1986).

[58] J. B. Gao, Phys. Rev. Lett. **83**, 3178 (1999).

[59] J. B. Gao and H. Q. Cai, Phys. Lett. A **270**, 75 (2000).

[60] S. A. Pawar, A. Seshadri, V. R. Unni, and R. I. Sujith, J. Fluid Mech. **827**, 664 (2017).

[61] T. Vicsek and A. Zafeiris, Phys. Rep. **517**, 71 (2012).

[62] N. B. George, V. R. Unni, M. Raghunathan, and R. I. Sujith, J. Fluid Mech. **849**, 615 (2018).

[63] R. I. Sujith and S. A. Pawar, *Thermoacoustic Instability* (Springer, Berlin, 2021).

[64] J. Feldhoff, R. Donner, J. Donges, N. Marwan, and J. Kurths, Phys. Lett. A **376**, 3504 (2012).

[65] Y. Guan, K. Moon, K. T. Kim, and L. K. B. Li, J. Fluid Mech. **938**, A5 (2022).

[66] H. Gotoda, M. Amano, T. Miyano, T. Ikawa, K. Maki, and S. Tachibana, Chaos **22**, 043128 (2012).

[67] J. Tony, E. A. Gopalakrishnan, E. Sreelekha, and R. I. Sujith, Phys. Rev. E **92**, 062902 (2015).

[68] H. Kobayashi, H. Gotoda, S. Tachibana, and S. Yoshida, J. Appl. Phys. **122**, 224904 (2017).

[69] H. Gotoda, H. Kobayashi, and K. Hayashi, Phys. Rev. E **95**, 022201 (2017).

[70] K. Takagi and H. Gotoda, Phys. Rev. E **98**, 032207 (2018).

[71] T. Tokami, T. Hachijo, T. Miyano, and H. Gotoda, Phys. Rev. E **101**, 042214 (2020).

[72] Y. Nomi, H. Gotoda, S. Kandani, and C. Almarcha, Phys. Rev. E **103**, 022218 (2021).

[73] Y. Nomi, H. Gotoda, S. Fukuda, and C. Almarcha, Chaos **31**, 123133 (2021).